

Article

# Self-Shattering Defect Detection of Glass Insulators Based on Spatial Features

Haiyan Cheng <sup>1</sup>, Yongjie Zhai <sup>1</sup>, Rui Chen <sup>1,\*</sup>, Di Wang <sup>2</sup>, Ze Dong <sup>1</sup> and Yutao Wang <sup>1</sup>

<sup>1</sup> Hebei Engineering Research Center of Simulation and Optimized Control for Power Generation, North China Electric Power University, Baoding 071003, China; chenghaiyan78@126.com (H.C.); zhaiyongjie@ncepu.edu.cn (Y.Z.); dongze33@126.com (Z.D.); 18730265696@163.com (Y.W.)

<sup>2</sup> Power China Guizhou Electric Power Design & Research Institute Co., LTD, Guiyang 550002, China; ncepuwangdi@163.com

\* Correspondence: cr\_chenrui@foxmail.com; Tel.: +86-136-6379-3681

Received: 21 January 2019; Accepted: 4 February 2019; Published: 10 February 2019



**Abstract:** During an automatic power transmission line inspection, a large number of images are collected by unmanned aerial vehicles (UAVs) to detect existing defects in transmission line components, especially insulators. However, with twin insulator strings in the inspection images, when the umbrella skirts of the rear string are obstructed by the front string, defect detection becomes difficult. To solve this problem, we propose a method to detect self-shattering defects of insulators based on spatial features contained in images. Firstly, the images are segmented according to the particular color features of glass insulators, and the main axes of insulator strings in the images are adjusted to the horizontal direction. Then, the connected regions of insulators in the images are marked. After that, the vertical lengths of the regions, the number of insulator pixels in the regions, as well as the horizontal distances between two adjacent connected regions are selected as spatial features, based on which defect discriminants are formulated. Finally, experiments are performed using the proposed formula to detect self-shattering defects in the insulators, using the spatial distribution of the connected regions to locate the defects. The experiment results indicate that the proposed method has good detection accuracy and localization precision.

**Keywords:** defect detection; glass insulator; localization; self-shattering; spatial features

## 1. Introduction

In recent years, the difficulty of conducting manual inspections on transmission lines has been increasing with the enlargement of transmission lines. In order to reduce the workload of inspection work and improve inspection efficiency, unmanned aerial vehicles (UAVs) are used for transmission line inspections [1–3]. During UAV inspections, a number of images are collected to detect the defects in transmission lines. The use of image detection technology greatly improves the efficiency and has become a research hotspot in current smart grids [4–7]. Insulators, of which the main roles are electrical insulation and line support, are very important components of transmission lines. Since glass insulators have the characteristics of zero value self-shattering, when an insulator is subjected to changes in terms of cold and heat, its compression stresses the surface and opposing tensile internal stresses become greater, which can cause breakdown easily. As a result, the insulation value at both ends of the insulator string becomes zero and the insulation function is lost. Therefore, zero value detection of insulators is required. When the insulation value is zero, a glass insulator will shatter, and it is easy to be found with visual detection. Additionally, because they are widely used in 500 kV high voltage transmission lines, detection of self-shattering defects in insulators has become a significant issue.

Therefore, many methods are suggested to detect self-shattering defects in glass insulators. They are as follows:

- (1) Detection method based on contour information. Some researchers [8–11] firstly identified the contours of insulators, and then determined whether there were self-shattering defects according to the relative distances between adjacent insulators. Nevertheless, the insulators will sometimes be obscured because of unsuitable shooting angles of cameras. In addition, the backgrounds of the aerial images are complex and changeable. Therefore, the contour extraction of insulators will be influenced and the accuracy of the above detection method is affected.
- (2) Detection method based on texture features. Zhang [12] and Wang [13] calculated the texture values of insulator images by block, and then analyzed whether the insulator was missing by comparing texture values. However, the calculation amounts of this method are very large. Zhang [14] obtained the directions of insulator strings by detecting parallel line segments. Then, the insulator string was divided into blocks according to the direction and the distance between the slices. After that the existence of self-shattering defects were judged by the similarity of texture features between the blocks. However, when the insulator pieces were obstructed or the shooting distance was large, the line features of the insulator pieces were very vague, which easily led to false detection.
- (3) Detection method based on histogram matching features. Lin [15] diagnosed glass insulator faults based on a histogram matching criterion and determined faultless insulators within a certain range. However, the method could not indicate the specific locations of the fault insulators. Shi [16] used a sliding window method to match the gray histogram of the insulators and the templates, and inferred and located insulator defects according to histogram distances. However, it was easily influenced by the detection environment and the selection of templates.
- (4) Detection method based on region features. Wang [17] segmented insulators in a lab color space and calculated the proportion of insulator pixels in each insulator region to determine the drop-off fault. Jiang [18] divided the insulator area into individual pieces, and judged the fault by sensing the distances between the gravity centers of adjacent insulator pieces. Nevertheless, when the insulator string was obstructed and the two insulator strings could not be separated completely, the detection accuracies of the two methods were influenced. Zhai [19] segmented insulator images in the RGB color space, and performed an adaptive morphology process on the images according to the area ratio of the insulator region. After that, the fault point was located. However, when the missing pieces were at the ends of the insulator string, they may have gone undetected.

The above-mentioned methods are mainly aimed at self-shattering defect detection of unobstructed glass insulators and have achieved good detection results within a certain range. However, in the process of transmission line inspections, insulators in the aerial images are often obstructed and also connected to each other because of the influence of the shooting distance and angle. Thus, most of the above methods show difficulty in obtaining the expected results.

Aiming at the above deficiencies and inspired by the literature [20], in this paper, we propose a self-shattering defect detection method for obstructed or unobstructed twin insulator string images based on the obvious spatial features of the insulator regions. The overall framework of this method is shown in Figure 1. The main technical contributions made in this work include: (1) For images of twin glass insulator strings, the self-shattering defect can be detected and the defect position can be located accurately, regardless of whether the insulators are obstructed or not; and (2) robustness and real-time performance is evaluated, and they may meet the requirements of strong robustness and high real-time performance demands of power line inspection. The remainder of this paper is organized as follows: In Section 2, the glass insulator image compound binarization processing are introduced. Then, in Section 3, the new detection and localization method of insulator self-shattering defects is described in detail. After that, in Section 4, experiments to verify the performance of the proposed method are explained. Finally, the conclusions are drawn in Section 5.

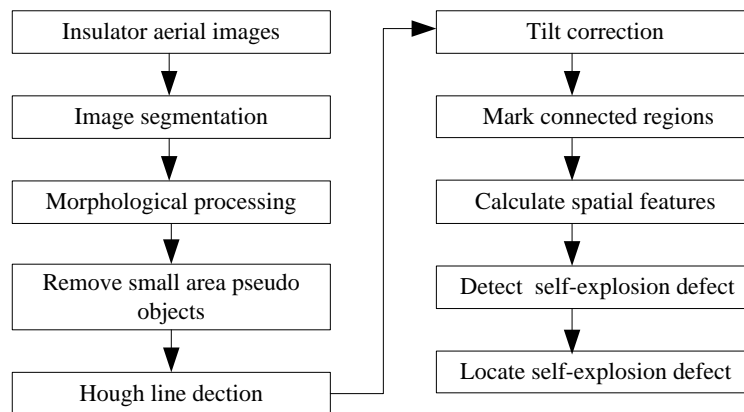


Figure 1. Flow chart showing the insulator self-shattering defect detection method.

## 2. Insulator Images Compound Binarization

The process of compound binarization mainly includes image segmentation, removal of pseudo targets and tilt correction.

### 2.1. Insulator Images Segmentation

Color is an intuitive feature of objects. Glass insulators without RTV spraying have a special color. It is generally green and very different to most background colors. Therefore, insulator images can be segmented according to their color features.

The authors of References [17,21] segmented insulator images using single thresholds in Lab space and HSI space, respectively. Because of the complex background in insulator images, it is difficult to achieve a good segmentation effect with a single threshold.

Inspection images collected by UAVs are usually RGB space images. In this paper, the R, G and B components of 150 glass insulator images were sampled, respectively, and their spatial distribution features were statistically analyzed. The color distribution rules of the glass insulators were as follows:

$$\begin{cases} 65 \leq R \leq 175 \\ 115 \leq B \leq 180 \\ 30 \leq G - R \leq 65 \end{cases} \quad (1)$$

where  $R$ ,  $G$  and  $B$  are the component values of red, green and blue, respectively.

The threshold values of the  $R$ ,  $G$  and  $B$  components are set by Equation (1). Thus, the glass insulators can be easily separated from the complex background. Figure 2 shows the segmentation results of aerial insulator images according to Equation (1). Although the backgrounds of the two images were both very complex, good segmentation results were obtained regardless of whether the insulators were obstructed or not.

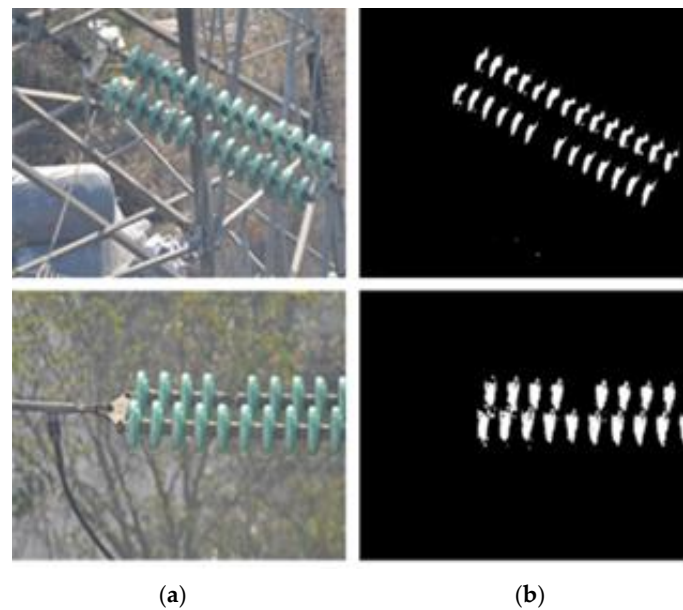


**Figure 2.** Results of segmentation: (a) Original aerial images; (b) Segmentation results.

### 2.2. Pseudo Objects Removal and Tilt Correction

After segmentation, the insulators images were separated from the background. However, there still existed some narrow breaks and small burrs in the images. Thus, the morphological closed operation and median filter were used to process the images [22]. After that, the small area pseudo objects were removed. Figure 3 shows the processing results of removal of the pseudo objects.

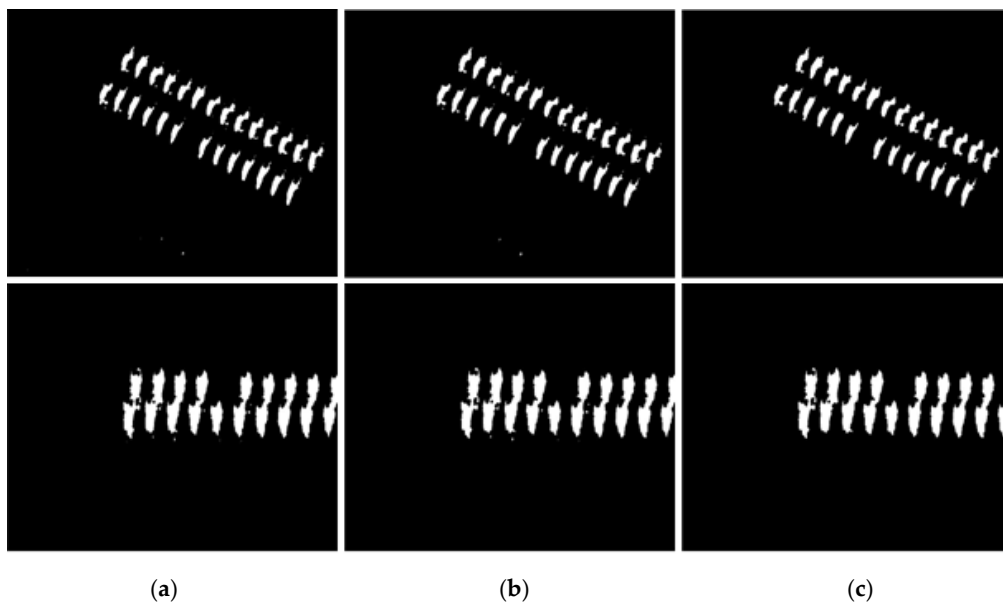


**Figure 3.** Pseudo objects removing process: (a) Morphological processing; (b) Median filter; (c) Pseudo objects removal.

Due to the influence of the shooting angle, insulators present different angles in the image. Thus, the image needs to be corrected to locate the main axis of the insulator string in the horizontal direction. Thus, it can make preparation for the spatial feature descriptions of the insulator regions. The direction of the longest line segment is the direction of the main axis of the insulator string in the image. Thus, the inclination angle of the main axis can be obtained using the Hough transform. According to the

angle, the insulator string axis can be rotated in the horizontal direction. Figure 4 shows the processing results of tilt correction.

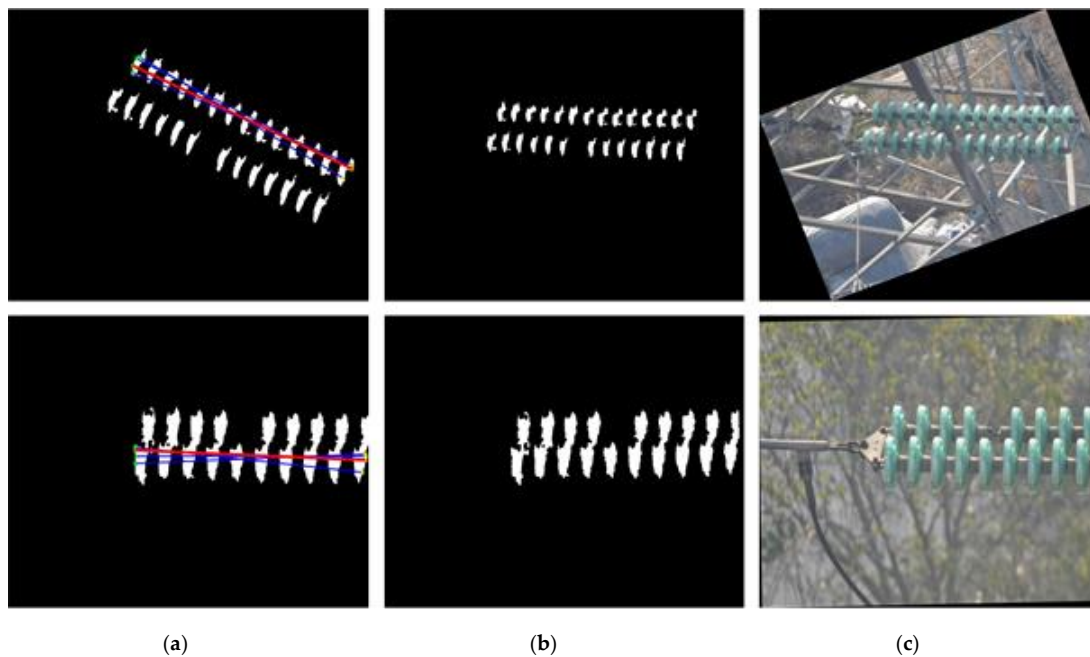


**Figure 4.** Tilt correction: (a) Hough transformation detection of lines; (b) Tilt correction; (c) Correction of original image.

It can be seen from Figures 3 and 4 that effective binarization images were obtained after image compound binarization. The contours of the insulators may be incomplete, but the spatial distribution of the insulator regions can be expressed regardless of if the insulators are obstructed or not.

### 3. Self-Shattering Defect Detection of Insulators

#### 3.1. Spatial Features Description of Insulators

An insulator string is composed of a main shaft and a certain number of insulators. The insulators are perpendicular to the main shaft. The insulators on the same string have the same shape, size and color, and the distances between the adjacent umbrella skirts of the insulators are equal. All these characteristics indicate that insulators have consistent spatial features.

In order to represent the spatial features, the connected regions of the binary images are marked. The connected regions of normal insulators have three obvious features: (1) the vertical lengths of each connected region are close; (2) the number of insulator pixels in the region varies little; and (3) the horizontal distances between adjacent connected regions are very similar. In addition, the numerical distributions of the above three values are relatively uniform, as shown in Figure 5a. In Figure 5, the first row contains inspection images, corresponding connected regions of insulators are given in the second row, and the vertical length, the number of insulator pixels and the horizontal distance are in the third to the fifth rows, respectively.

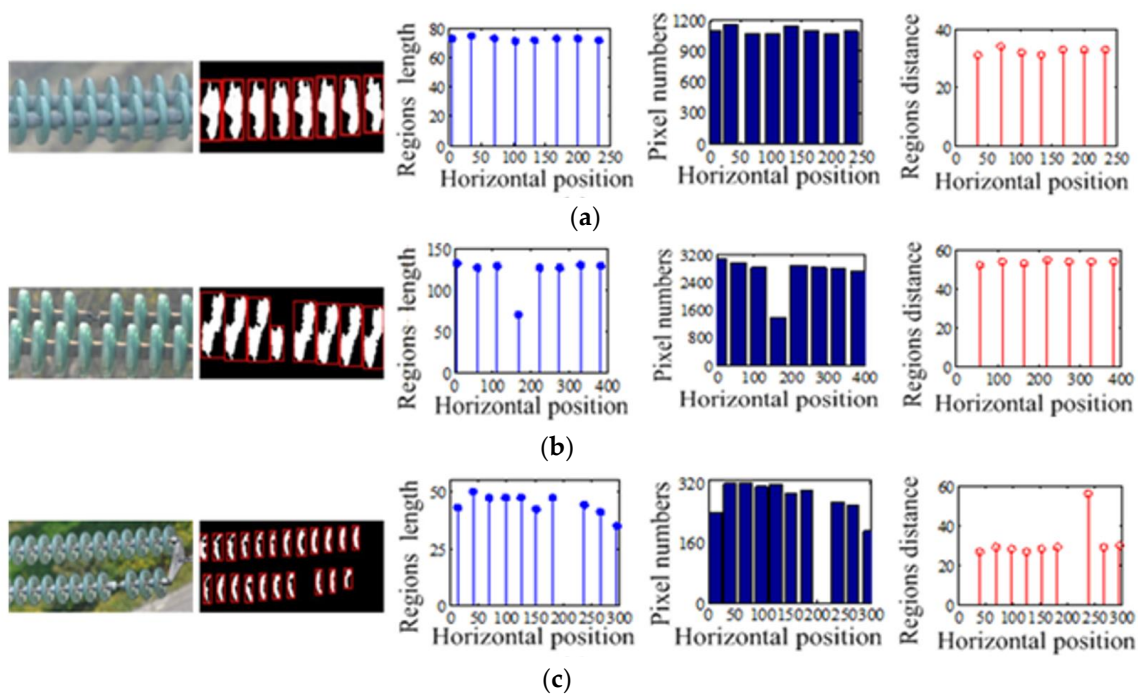


**Figure 5.** Spatial features of connected regions: (a) Normal; (b) Self-shattering with obstruction; (c) Self-shattering without obstruction.

When a self-shattering defect occurs, the spatial consistency of the insulator regions is destroyed, and spatial features change significantly. There are generally two cases of spatial locations of the twin insulator strings in the images. One is that the front string obstructs the back one, and the twin strings cannot be divided into individual strings in the image. Another situation is that the two insulator strings are not obstructed by each other, thus they can be separated into two strings. In the first situation, when the self-shattering defect occurs, the vertical lengths and the numbers of insulator pixels of the connected region are obviously smaller than those in the normal regions. Additionally, the numerical values are abruptly changed, as shown in Figure 5b. In the second situation, two insulator strings can be treated separately. When the self-shattering defect occurs, the horizontal distance between the connected regions on both sides of the defective insulator is obviously greater than those of other adjacent regions, and there is a clear jump, as shown in Figure 5c (Figure 5c presents the spatial features of the insulator string on which self-shattering occurs).

As can be seen from Figure 5, the spatial features of the self-shattering insulators are very different from the normal insulators. Therefore, the self-shattering defect can be discriminated according to the vertical lengths of the connected region, the number of insulator pixels in the region, and the horizontal distances between the adjacent regions.

### 3.2. Self-Shattering Defect Detection

#### 3.2.1. Spatial Features Determination of Insulator Connected Regions

Following the above image processing, the main axis of the insulator string has been tilted in the horizontal direction. Then, the connected regions of the insulators are located using the 8-adjacency connected region method. For convenience of description, the connected region of each insulator is described by a four-dimensional vector  $(x, y, w, h)$ . Where  $x$  and  $y$  correspond to the start point coordinates of the connected region on the x-axis and y-axis with the origin at the upper left corner, and  $w, h$  represent the horizontal width and vertical length of the region, respectively.

Based on analysis of the insulator spatial features, three spatial features, which characterize the connected regions of the insulators, are constructed as follows:

- (1) Vertical length  $h_i$ : The vertical length of the connected region of the  $i - th$  insulator.
- (2) Number of insulator pixels  $n_i$ : The area of the connected region of the  $i - th$  insulator.
- (3) Horizontal distance between two adjacent connected regions  $D_i$ :

$$D_i = |x_{i+1} - x_i|; i = 1, 2, \dots, k - 1 \quad (2)$$

where  $k$  is the number of connected regions,  $x_i$  is the horizontal coordinate of the starting point of the  $i - th$  connected region.

### 3.2.2. Self-Shattering Defect Discriminant Definition

After determining the three spatial features of the insulators connected regions, self-shattering defect discrimination can be performed. Corresponding to the former two insulator string location situations, through statistical analysis, the discriminant<sub>1</sub> and discriminant<sub>2</sub> are summarized respectively in Equations (3) and (4):

$$\text{discriminant}_1 : \begin{cases} h_i \leq 0.7\bar{h} \\ n_i \leq 0.58\bar{n} \end{cases}; i = 1, 2, \dots, k \quad (3)$$

where  $\bar{h}$  and  $\bar{n}$  are the average of  $h$  and  $n$ , respectively.

$$\text{discriminant}_2 : D_i > 1.7\bar{D}; i = 1, 2, \dots, k - 1 \quad (4)$$

where  $\bar{D}$  is the average of  $D$ .

When discriminant<sub>1</sub> or discriminant<sub>2</sub> is satisfied, it can be concluded that insulator self-shattering has occurred.

### 3.2.3. Self-Shattering Defect Localization

When the spatial features of the twin insulator strings satisfy discriminant<sub>1</sub>, the latter insulator string is obstructed, and self-shattering may occur in either string. Thus, the defect location can be obtained by Equations (5)–(8).

$$x_{fault} = x_i \quad (5)$$

$$y_{fault} = \begin{cases} 0.5(y_{i-1} + y_{i+1}); y_i \gg \bar{y} \\ y_i + h_i; y_i \approx \bar{y} \end{cases} \quad (6)$$

$$w_{fault} = 0.5(w_{i-1} + w_{i+1}) \quad (7)$$

$$h_{fault} = 0.5(h_{i-1} + h_{i+1}) - h_i \quad (8)$$

where  $\bar{y}$  is the average of  $y$ . For special cases, when self-shattering occurs at both ends of an insulator string, Equation (9) is used:

$$y_{i+1} = y_{i-1}, w_{i+1} = w_{i-1}, h_{i+1} = h_{i-1} \quad (9)$$

When the spatial features of the twin insulator strings satisfy discriminant<sub>2</sub>, the insulators are not obstructed by each other. Thus, Equations (10)–(13) are adopted to calculate the defect location coordinates:

$$x_{fault} = x_i + 0.5D_i \quad (10)$$

$$y_{fault} = 0.5(y_i + y_{i+1}) \quad (11)$$

$$w_{fault} = 0.5(w_i + w_{i+1}) \quad (12)$$

$$h_{fault} = 0.5(h_i + h_{i+1}) \quad (13)$$

When there is no overlap between the twin insulator strings, they will be processed separately. In this case, if self-shattering occurs at both ends of one insulator string, the self-shattering defect can be judged based on the difference between the connected region numbers of the two insulator strings.

Figure 6 shows a flow chart of the self-shattering defect detection process after image compound binarization.

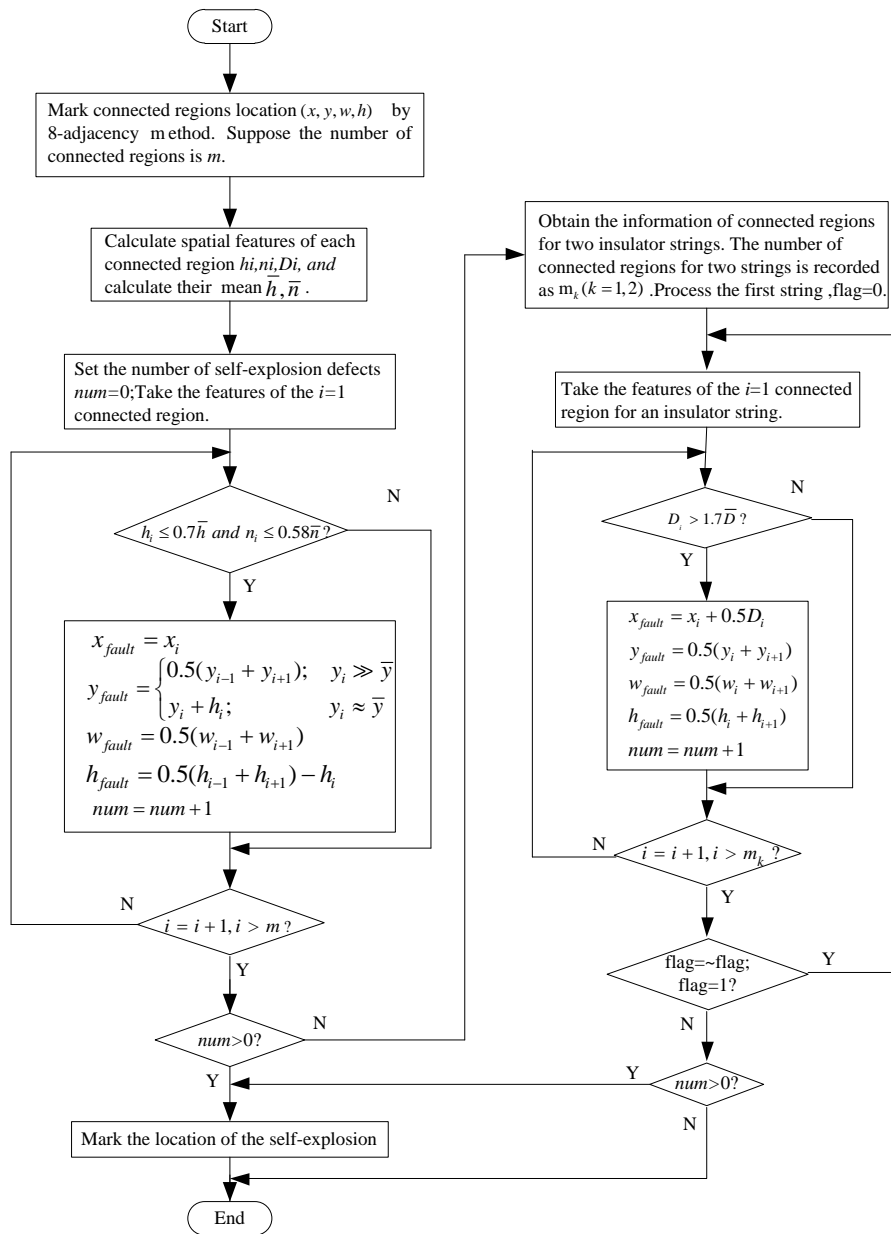


Figure 6. Flow chart of the proposed detection method.

When the back insulators are obstructed, the main pseudo code of the self-shattering detection is as follows (Algorithm 1):

**Algorithm 1.** Self-shattering detection process with obstructed.**Input:** binarization image bwsrc**Output:** Self-shattering location

```

1: [B, num] = bwlabel(bwsrc, 8);
2: box = regionprops(B, 'BoundingBox', 'Area');
3: areas = [box.Area];
4: rects = cat(1, box.BoundingBox);
5: avgarea = mean(areas(:));
6: [m, n] = size(rects);
7: x = rects(:, 1); y = rects(:, 2);
8: w = rects(:, 3); h = rects(:, 4);
9: avgy = mean(y); avgh = mean(h);
10: hnorm = 0.7 * avgh; anorm = 0.58 * avgarea;
11: num = 0;
12: for j = 1 to m do
13:   if h(j) <= hnorm & areas(j) <= anorm
14:     num = num + 1;
15:     xx(num) = x(j);
16:     ww(num) = 0.5 * (w(j - 1) + w(j + 1));
17:     hh(num) = 0.5 * (h(j - 1) + h(j + 1)) - h(j);
18:   if abs(y(j) - avgy) <= 10
19:     yy(num) = y(j) + h(j);
20:   else yy(num) = 0.5 * (y(j - 1) + y(j + 1));
21:   end if
22: end if
23: end for
24: for k = 1 to num do
25:   rec tan gle('position', [xx(k), yy(k), ww(k), hh(k)]);
26: end for

```

The self-shattering location detected by the proposed method is illustrated in Figure 7.

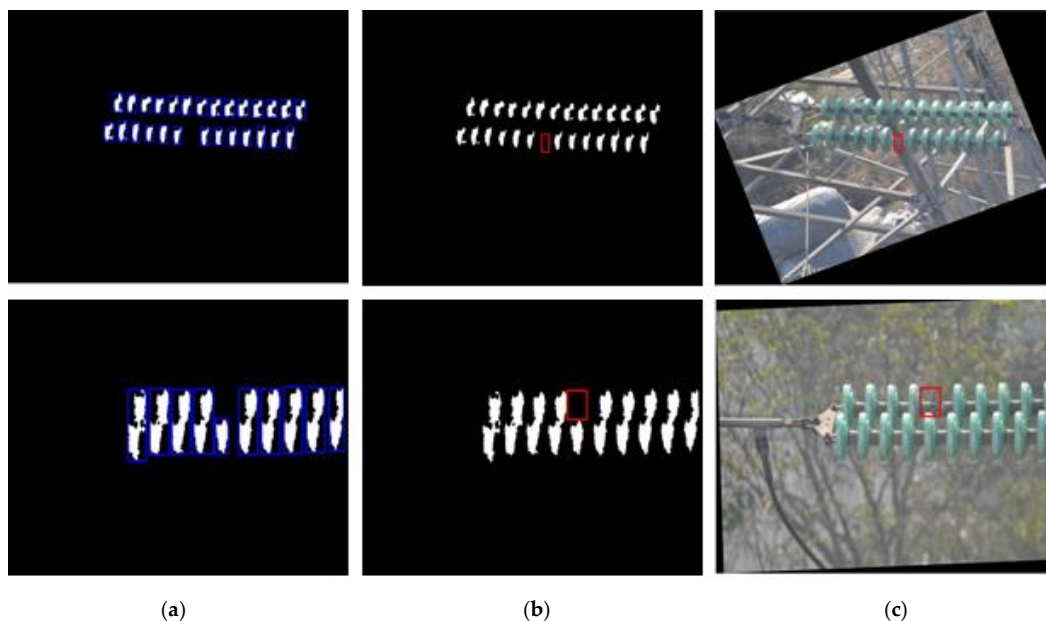


**Figure 7.** Results of localization: (a) Connected regions of insulators; (b) Self-shattering location; (c) Localization of original image.

## 4. Experimental Results and Analysis

### 4.1. Self-Shattering Detection and Localization Results Analysis

Experiments were conducted to evaluate the proposed method with real inspection images collected by UAVs. The experiment environments included the Windows 7 operating system with a CPU main frequency of 3.40 GHz, 4.00 GB RAM, and MATLAB 2015b. Figure 8 presents a part of the experimental results. The results show that the proposed method efficiently detected and located the insulator self-shattering defects.

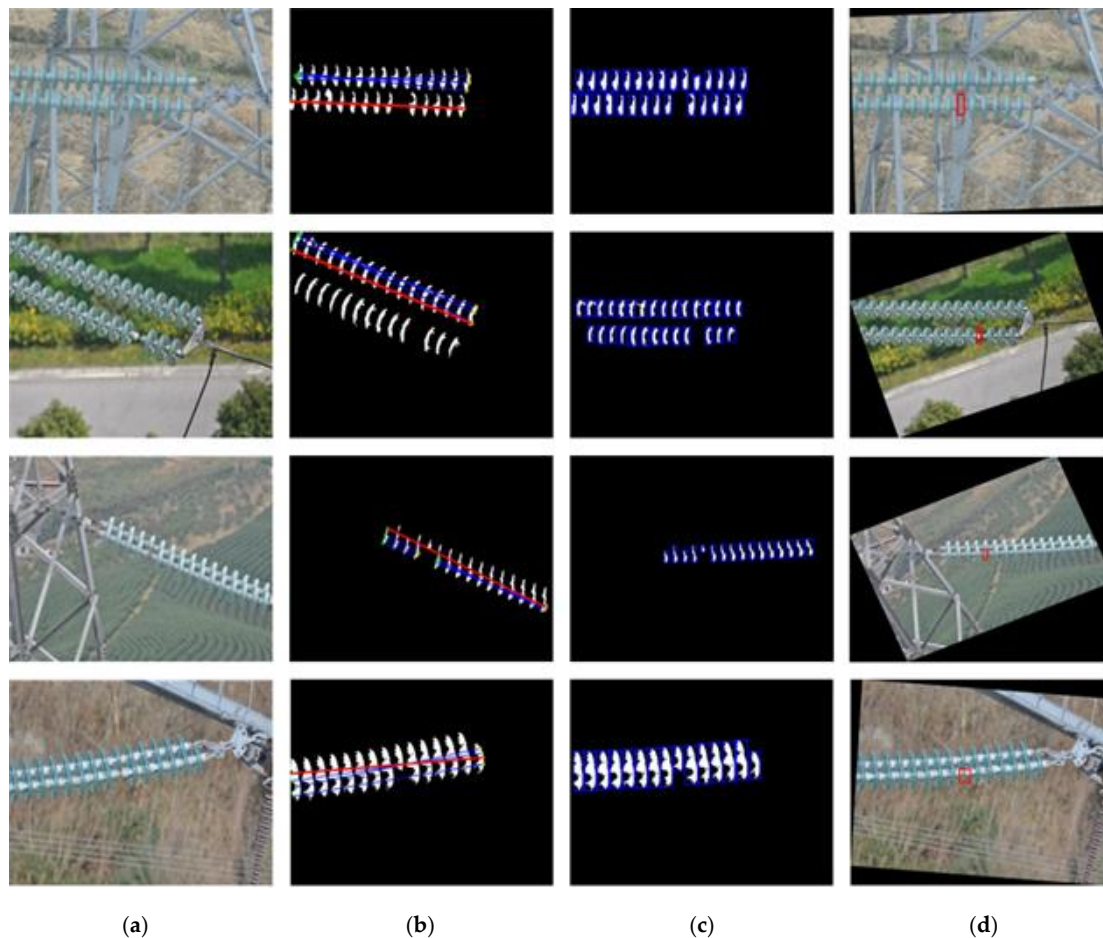


**Figure 8.** Test results: (a) Original image; (b) Detected lines; (c) Connected regions; (d) Defect localization.

### 4.2. Robustness Analysis

In this section, the robustness of the proposed method is analyzed through comparison with existing insulator self-shattering defect detection methods.

#### 4.2.1. Detection Effect under Different Obstructed Conditions

The detection effect of the proposed method was compared with the methods in the literature [17,19,23] for inspection images with different obstruction conditions. The results are shown in Figures 9 and 10. It can be seen that the proposed method accurately located the self-shattering defects of the insulators in both conditions, and had strong robustness.

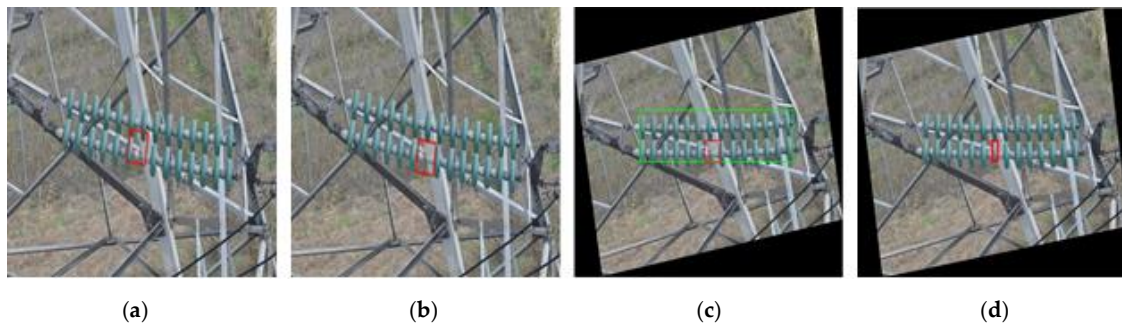


**Figure 9.** Comparison for insulators under the individual condition: (a) Literature [17] method; (b) Literature [19] method; (c) Literature [23] method; (d) Proposed method.

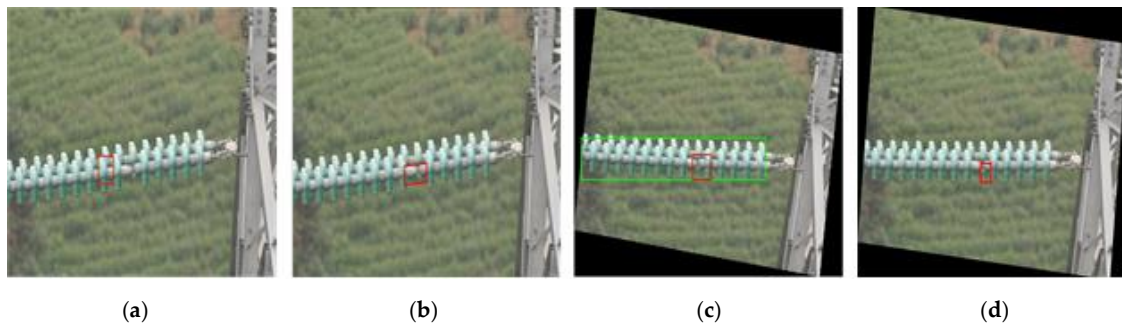


**Figure 10.** Comparison for insulators under the obstructed condition: (a) Literature [17] method; (b) Literature [19] method; (c) Literature [23] method; (d) Proposed method.

#### 4.2.2. Detection Effects of Images with Different Background Complexities

The difficulty of self-shattering defect detection was different with different background complexities. The inspection images with different background complexities were used to further evaluate the performance of the proposed method. Experimental results are shown in Figure 11. It is demonstrated that the proposed method accurately located the self-shattering defects in inspection images with simple backgrounds and complex backgrounds.

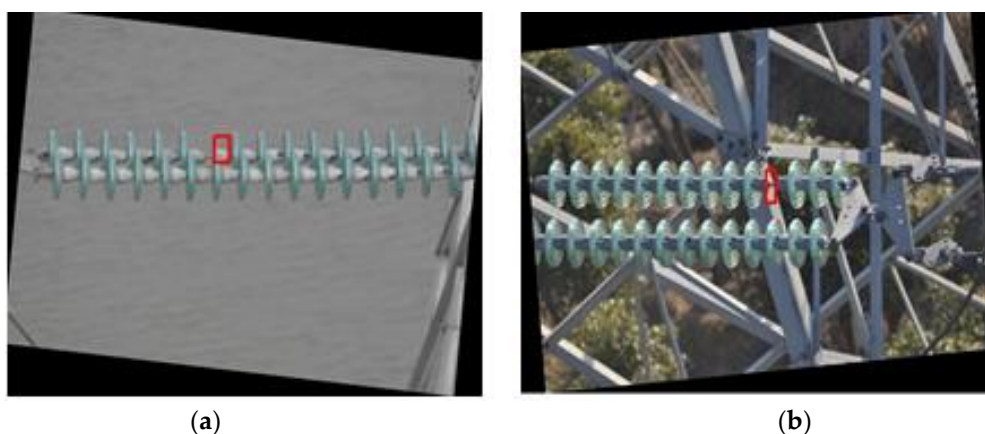


**Figure 11.** Results under different background complexities: (a) Simple background; (b) Complex background.

#### 4.2.3. Self-Shattering Occurs at Both Ends of the Insulator String

The methods proposed in Reference [17,19] were not applicable for the situation where self-shattering occurs at both ends of one insulator string. However, the experimental results of

the proposed method and the method used in Reference [23] are illustrated in Figure 12. It can be observed that literature [23] method got false self-shattering location, and the proposed method detected the self-shattering defect at one end of the insulator string, whereas it misjudged the visual vacancy on the other end, which led to error detection. From an operation and maintenance point of view, missed detection may lead to missing a fault, which can cause safety risks, while false detection may increase the workload of the secondary judgment. When the missed detection and the false detection cannot be completely avoided, in contrast, the choice is false detection rather than missed detection to improve safety. Therefore, the proposed method is more suitable for practical needs.

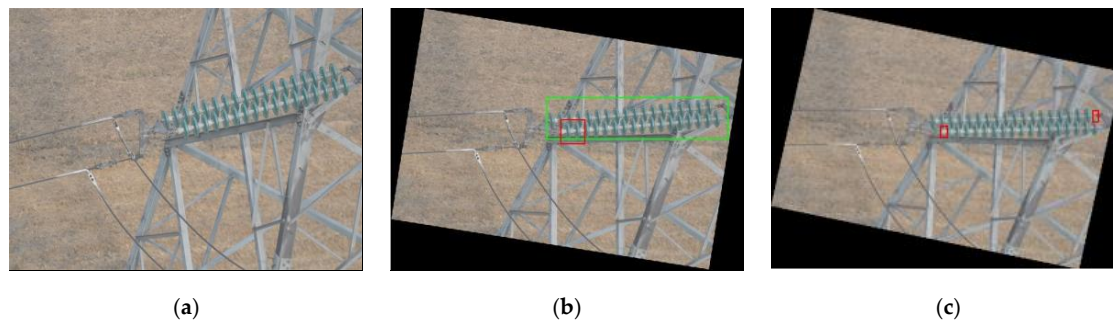


**Figure 12.** Detection result of self-shattering located at the end of insulator string: (a) Original image; (b) Literature [23] method; (c) Proposed method.

According to the above analysis, we conclude that the proposed method accurately detected and located the self-shattering defect of insulators in inspection images with different obstructed conditions, different self-shattering positions and different background complexities, which means that the proposed method had strong robustness.

#### 4.3. Real-Time Performance and Precision

In order to analyze the real-time performance and detection precision of the proposed method, 67 inspection images of insulators with self-shattering defects were detected. The average time consumption, precision and missing rate were used as evaluation indexes. They are defined in Equations (14) and (15):

$$\text{precision} = TP / (TP + FP) \quad (14)$$

$$\text{missing rate} = FN / (TP + FN) \quad (15)$$

where  $TP$  represents the number of correctly located self-shattering insulators,  $(TP + FP)$  is the total number of located self-shattering insulators,  $FN$  represents the number of undetected self-shattering insulators, and  $(TP + FN)$  is the total number of self-shattering insulators.

The performances of the proposed method were compared with the methods in References [17,19,23], as shown in Table 1.

**Table 1.** Comparison of performances of proposed method with methods in References [17,19,23].

Method	Precision (%)	Missing Rate (%)	Average Time Consumption (s)
literature [17]	63.8	15.2	1.95
literature [19]	91.04	8.58	0.52
literature [23]	91.79	7.86	0.68
Proposed Algorithm	92.54	7.13	0.58

It was observed that the proposed method in this paper was superior to the method in References [17,23], which reduced the average time consumption and the missing rate of detection,

and improved detection precision. Furthermore, compared with the method proposed in Reference [19], although our method took a slightly longer time, it had a higher precision and lower missing rate, which is more in line with actual needs.

## 5. Conclusions

In this paper, a detection and localization method for self-shattering defects in twin glass insulators, based on spatial features of connected regions, was proposed. In our method, firstly, the insulators in the inspection images were segmented from complex backgrounds based on color features, then insulator connected regions were marked, and finally insulators with defects could be detected and located based on spatial features. The performance of the proposed method was evaluated using inspection images under different conditions. Experimental results confirm that this method is simple, effective, and has a wide application range as well as good real-time performance.

In addition, when insulator regions are severely obstructed, an independent connected region based on the insulator umbrella skirt cannot be obtained, which results in poor performance of the method. Thus, further research based on spatial features is needed for the localization and detection of multiple and simultaneous bunch-drop faults in insulators.

**Author Contributions:** H.C., Y.Z., and Z.D. designed the system modeling and algorithm; H.C. and R.C. performed the experiments; H.C. and D.W. analyzed the experimental results; H.C., Y.Z., R.C. and Y.W. wrote this paper.

**Funding:** This study is supported by National Natural Science of Foundation of China (61773160, 61871182), and National Natural Science Foundation of Hebei Province (F2017502016).

**Conflicts of Interest:** The authors declare no conflicts of interest.

## References

- Peng, X.; Qian, J.; Wang, K. Multi-sensor full-automatic inspection system for large unmanned helicopter and its application in 500 kv lines. *Guangdong Electr. Power* **2016**, *29*, 8–15.
- Wang, M.; Du, Y.; Zhang, Z. Research on UAV aided inspection and image recognition of insulator defects. *J. Electron. Meas. Instrum.* **2015**, *29*, 1862–1869.
- Guan, Z.; Wang, X.; Bian, X.; Wang, L.; Jia, Z. Analysis of causes of outdoor insulators damages on HV and UHV transmission lines in China. In Proceedings of the IEEE Electrical Insulation Conference, Philadelphia, PA, USA, 8–11 June 2014; pp. 227–230. [[CrossRef](#)]
- Liao, S.; An, J. A robust insulator detection algorithm based on local features and spatial orders for aerial images. *IEEE Geosci. Remote Sens. Lett.* **2015**, *12*, 963–967. [[CrossRef](#)]
- Cui, J.; Cao, Y.; Wang, W. Application of an improved algorithm based on watershed combined with krawtchouk invariant moment in inspection image processing of substations. *Proc. CSEE* **2015**, *35*, 1329–1335. [[CrossRef](#)]
- Zhao, Z.; Xu, G.; Qi, Y.; Liu, N.; Zhang, T. Multi-patch deep features for power line insulator status classification from aerial images. In Proceedings of the International Joint Conference on Neural Network (IJCNN), Vancouver, BC, Canada, 24–29 July 2016; pp. 3187–3194. [[CrossRef](#)]
- Yang, L.; Jiang, X.; Hao, Y.; Li, L.; Li, H.; Li, R.; Luo, B. Recognition of natural ice types on in-service glass insulators based on texture feature descriptor. *IEEE Trans. Dielectr. Electr. Insulation* **2017**, *24*, 535–541. [[CrossRef](#)]
- Jiang, H.; Jin, L.; Yan, S. Recognition and fault diagnosis of insulator string in aerial images. *J. Mech. Electron. Eng.* **2015**, *32*, 274–278.
- Zhang, S.; Yang, Z.; Huang, X.; Wu, H.Q.; Gu, Y.Z. Defects detection and positioning for glass insulator from aerial images. *J. Terahertz Sci. Electron. Inf. Technol.* **2013**, *11*, 609–613.
- Shang, J.; Li, C.; Chen, L. Location and detection for self-explode insulator based on vision. *J. Electron. Meas. Instrum.* **2017**, *31*, 844–849.
- Oberweger, M.; Wendel, A.; Bischof, H. Visual recognition and fault detection for power line insulators. In Proceedings of the 19th Computer Vision Winter Workshop, Krtiny, Czech Republic, 3–5 February 2014; pp. 1–8.

12. Zhang, X.; An, J.; Chen, F. A method of insulator fault detection from airborne images. In Proceedings of the 2nd WRI Global Congress on Intelligent Systems, Wuhan, China, 16–17 December 2010; pp. 200–203. [[CrossRef](#)]
13. Wang, W.; Wang, Y.; Han, J. Recognition and drop-off detection of insulator based on aerial image. In Proceedings of the 9th International Symposium on Computational Intelligence and Design, Hangzhou, China, 10–11 December 2016; pp. 162–167. [[CrossRef](#)]
14. Zhang, J.; Han, J.; Zhao, Y. Insulator recognition and defects detection based on shape perceptual. *J. Image Graphi.* **2014**, *19*, 1194–1201.
15. Lin, J.; Han, J.; Chen, F.; Xu, X.; Wang, Y. Defects detection of glass insulator based on color image. *Power Syst. Technol.* **2011**, *35*, 127–133.
16. Shi, L. The Method of Image Detection on Defect Insulator in Transmission Line. Master's Thesis, Department of Control Engineering, North China Electric Power University, Beijing, China, March 2013.
17. Wang, Y.; Yan, B. Vision based detection and location for cracked insulator. *Comput. Eng. Design* **2014**, *35*, 583–587.
18. Jiang, Y.; Han, J.; Ding, J. The identification and diagnosis of self-blast defects of glass insulators based on multi-feature fusion. *Electr. Power* **2017**, *50*, 52–58.
19. Zhai, Y.; Wang, D.; Zhang, M.; Wang, J.; Guo, F. Fault detection of insulator based on saliency and adaptive morphology. *Multimed. Tools Appl.* **2017**, *76*, 12051–12064. [[CrossRef](#)]
20. Zhai, Y.; Wang, D.; Zhao, Z.; Cheng, H. Insulator string location method based on spatial configuration consistency feature. *Proc. CSEE* **2017**, *37*, 1568–1577. [[CrossRef](#)]
21. Yao, C.; Jin, L.; Yan, S. Recognition of insulator string in power grid patrol images. *J. Syst. Simul.* **2012**, *24*, 1818–1822.
22. Jia, L.; Song, S.; Yao, L.; Li, H.; Zhang, Q.; Bai, Y.; Gui, Z. Image denoising via sparse representation over grouped dictionaries with adaptive atom size. *IEEE Access* **2017**, *5*, 22514–22529. [[CrossRef](#)]
23. Zhai, Y.; Chen, R.; Yang, Q.; Li, X.; Zhao, Z. Insulator fault detection based on spatial morphological features of aerial images. *IEEE Access* **2018**, *6*, 35316–35326. [[CrossRef](#)]



© 2019 by the authors. Licensee MDPI, Basel, Switzerland. This article is an open access article distributed under the terms and conditions of the Creative Commons Attribution (CC BY) license (<http://creativecommons.org/licenses/by/4.0/>).